Chapter 1

Introduction

The central idea of femtochemistry [1, 2, 3, 4, 5] is the preparation of molecular (*e.g.* vibrational) wave packets and the detection of their motion in real time. Vibrational periods of small molecules are in the range of several hundreds of femtoseconds[1]; consequently, pulses in the femtosecond regime, which have been experimentally available since the mid eighties, are required for the investigation of vibrational dynamics. A special technique of femtosecond chemistry is the so-called pump-probe spectroscopy, in which the time evolution of elementary reaction steps can be observed by means of two ultrashort laser pulses acting like a stop-watch (pump-pulse = "start", probe-pulse = "stop"). These ultrashort techniques are used not only for analysing chemical reactions, but also for controlling reactions and competing processes [6, 7, 8, 9, 10].

Various approaches have been designed for controlling systems that have well characterized potential energy surfaces, dipole couplings, or other properties relevant for the laser driven reaction [11, 12, 13, 14, 15]. Some of these concepts have been verified for small *i.e.* typically di- or triatomic molecules [15, 16]. For more complex systems, Rabitz and Judson have suggested an ingenious alternative approach, adaptive optimal laser pulse control [17]. Essentially, this method teaches a laser pulse sequence to prepare specific products based on "fitness" information *e.g.* product yields provided by an adequate laboratory measurement device. Over a series of generations, the algorithm learns an optimal laser pulse for preparing the desired target. The experimental apparatus, which consists of a laser, a sample of molecules, and a measurement device, then acts as an analog computer that solves Schrödinger's equation exactly, for the optimal laser pulse in real time. This general method has been verified experimentally first by the group

---

[1]For instance, the vibrational period T_{osc} of the [CpMn(CO)$_2$]-CO (pseudo-diatomic) stretching vibration is 84 fs , calculated using the relation $T_{osc} = \frac{\lambda}{c_0}$, where c_0 is the speed of light and $\frac{1}{\lambda} = 396 \ cm^{-1}$ is the reciprocal wavelength numerically calculated by the Fourier Grid Hamiltonian Method (see chapter 2).

of Gerber [18, 19] with applications to the selective photoionization and photo-dissociation of ligands from organometallics [18], as well as by other groups see *e.g.* [20, 21, 22, 23, 24]. However, this method does not provide any direct information about the underlying mechanism of the laser driven reaction, except for some rather intuitive working hypotheses which the optimal laser pulse may suggest *e.g.* [24, 25, 26]. The purpose of this work is to explain for the first time the mechanism of the pump-probe experiments and adaptive optimal laser pulse control experiments on the "parent" ion, $CpMn(CO)_3^+$, competing against the the preperation of the "daughter" ion, $CpMn(CO)_2^+$, performed by the group of Wöste (Freie Universität Berlin) [24, 27, 28].

In order to simulate these experiments, *ab initio* quantum chemical calculations of the potential energy curves and transition dipole moments were performed first. The nonadiabatic couplings have been calculated numerically using the CI and MO coefficients of the *ab initio* electronic wave functions. Next, the nuclear dynamics is described by wave packet propagations on the *ab initio* potentials which are coupled by the laser pulses depending on the *ab initio* transition dipole moments and by the nonadiabatic couplings. As long as the studied processes occur on a time scale of a few hundred femtoseconds, intramolecular vibrational-energy redistribution (IVR) can be neglected. According to Trushin et. al. [29] dissociation channels via triplet states of organometallic compounds only play a role on time scales larger than 300 fs. Therefore, a one-dimensional description of the Mn-CO bond cleavage including only singlet electronic states is a valid approach and, consequently, this work is centered on the detailed dynamics of the decisive, dissociative metal-ligand bond.

Transition metal complexes play a major role in catalysis, in which they are involved in the homogeneous synthesis of various organic chemicals [30]. A considerable number of theoretical studies has investigated the electronic structure and nuclear dynamics of transition metal compounds, see for instance [31, 32, 33, 34, 35, 36]. The electronic structure of the ground state of $CpMn(CO)_3$ was previously explored at the Hartee-Fock level of theory and by photoelectron spectroscopy [37, 38].

Structure of the thesis

This work is organized as follows. This introduction (chapter 1) continues with some basic concepts concerning electronic transitions and photodissociation, the presentation of some experimental results, and the description of the one-dimensional model used in this work.

The nuclear dynamics simulations of this work are based on *ab initio* potential energy curves. Hence, chapter 2 reviews the basic ideas and equations of quantum dynamical wave packet propagation, paying special attention to the adiabatic and

diabatic representation of the nuclear dynamics. Furthermore, we describe the applied quantum chemical *ab initio* and *density functional* methods used to solve the electronic problem. Additionally, the estimation of the kinetic coupling using the *ab initio* electronic wave functions is explained.

In chapter 3, the calculated geometries of the ground and low-lying singlet excited states, vertical excitation spectra, *ab initio* potentials and transition dipole moments are presented. In the final part of this quantum chemical chapter the kinetic couplings are reported.

Following these quantum chemistry calculations chapter 4 deals with the quantum dynamical results of single pulse excitations to the excited states which are then probed with a second pulse. The resulting pump-probe simulations will be used to explain recent pump-probe and control experiments performed by the Wöste and coworkers (see above), which is the ultimate goal of this work.

Finally, the work is summarized with an outlook in chapter 5.

1.1 Basic concepts

1.1.1 Electronic transitions

In a one-electron picture, the molecular orbitals (MOs) can be used to describe the different electronic states involved in the electronic transitions. Qualitative molecular orbital theory describes chemical reactions in terms of the ground state electronic structure, for instance originating from a Hartree-Fock (see chapter 2) calculation. This is an approximation since the electronic wave function changes during a chemical reaction or an electronic transition. However, as long as the molecular orbital changes are small this qualitative picture can serve as a first approximation of intuitive schemes which can be visualized.

In this simplified MO scheme, the various electronic excitations of organo-transition metal complexes can be classified as follows [39]. Ligand field (LF) or d-d transitions do not change the charge on the central atom but occupy anti-bonding states, which can weaken ligand bonds and lead to dissociation. In contrast to LF excitations, the Charge-Transfer (CT) transitions change the electronic distribution between the metal atom and the ligands. CT states include Ligand-to-Metal- (LMCT), Metal-to-Ligand (MLCT) and Ligand-to-Ligand (LLCT) charge transfer states.

A Singlet-to-Singlet LF-transition corresponding to a "spin allowed" Absorption (A) is shown in figure 1.1. Other physical radiative processes include "forbidden" singlet-triplet absorption, "allowed" singlet-singlet emission (= Fluorescence (F)) and "forbidden" triplet-singlet emission (= Phosphorescence (P)). The
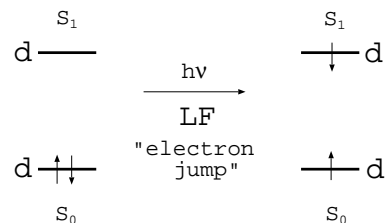
Figure 1.1: *Ligand field (LF) singlet-singlet transition.* S_0 = *singlet electronic ground state.* S_1 = *lowest electronic singlet excited state.*

commonly encountered photophysical <u>radiationless</u> processes are "allowed" transitions between states of the same spin (=Internal Conversion (IC)) and "forbidden" transitions between states of different spin (= Intersystem Crossing (ISC)) [40]. The time scale of the latter two types of transitions are of the order of 10^{-8} to 10^{-15} s. These processes are illustrated in the Jablonsky-type diagram of figure 1.2.
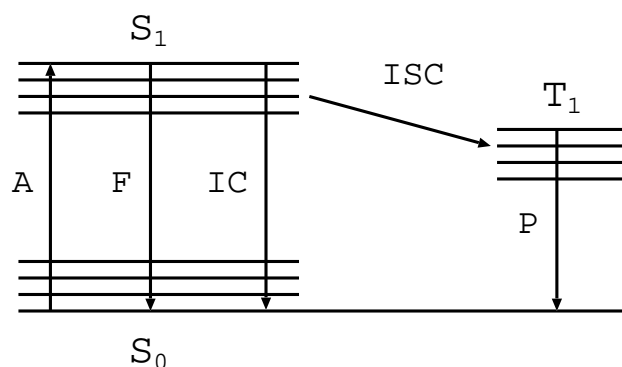

Figure 1.2: *Jablonsky diagram: A = Absorption, F = Fluorescence, IC = Internal Conversion, ISC = Intersystem Crossing, P = Phosphorescence.* S_0 = *ground, singlet state,* S_1 = *lowest excited, singlet state,* T_1 = *lowest triplet state.*

1.1.2 Types of photodissociation

Let us consider a diatomic molecule with atoms A and B or a pseudodiatomic molecule with fragments A and B. Formally, photodissociation consists of two subsequent steps [41]: The molecule is first transferred into an excited complex (AB)* by absorption of one or several photons:

$$AB + h\nu \rightarrow (AB)^* \text{ (Absorption).} \tag{1.1}$$

In a second step this complex decays in an unimolecular process leading to the fragments A and B:

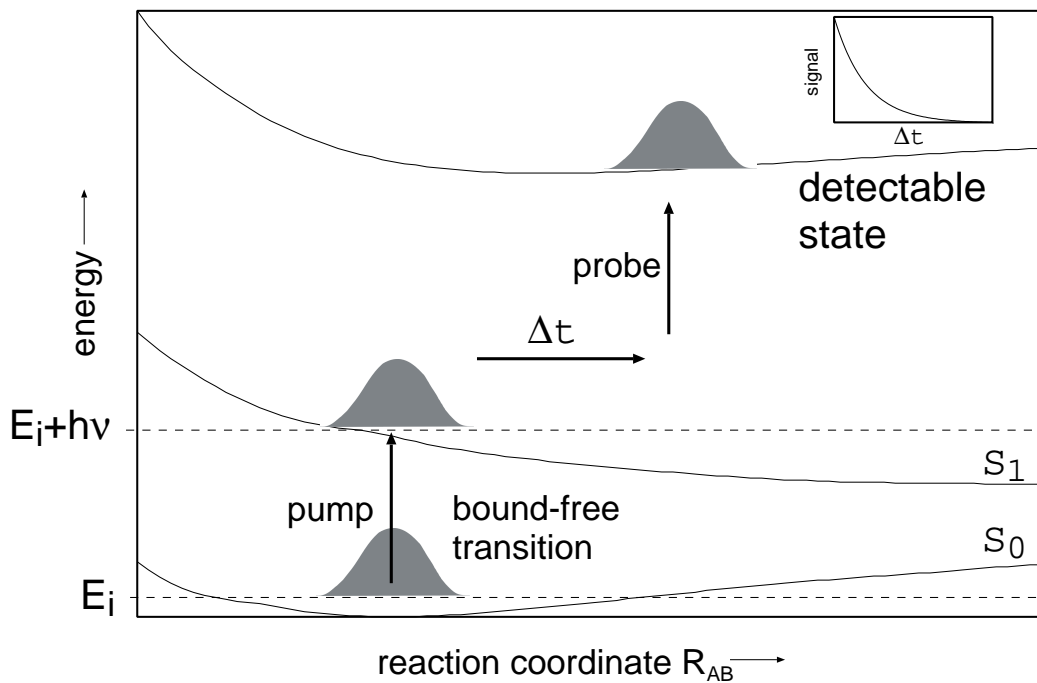$$(AB)^* \rightarrow A + B \text{ (Unimolecular decay).} \tag{1.2}$$

Figure 1.3: *Direct Photodissociation and measured exponentially decaying pump-probe signal as a function of the delay Δt (E_i = initial energy, $h\nu$ = pump photon energy).*

There are two basic types of photodissociation: A molecule may be dissociated by Infrared (IR) light. In that case many IR photons are necessary to excite the molecule from the vibrational ground state of the electronic ground state to an ensemble of quantum states above the dissociation threshold. This ensemble has a distribution of energies making an averaging over many quantum states unavoidable in a theoretical description. Since this first type, so-called *multiphoton dissociation*, which takes place in the electronic ground state, is not applied in this work, it is not further discussed here.

The second basic type, applied in this thesis, is ultraviolet (UV) photodissociation: The molecule is excited from the ground to an electronic excited state by a single (or several) UV (or visible) photon(s) with energy $h\nu$ (pump laser). If the potential of the upper electronic state is repulsive the excited complex (AB)* ultimately decays. This type of UV photodissociation - shown in figure 1.3 - is called direct photodissociation. In simple cases, the decay of the excited species with time t can be described by an exponential function:

$$[(AB)^*](t) = [(AB)^*](t = 0) \cdot e^{-\frac{t}{\tau}}, \tag{1.3}$$

where τ is the decay time. This decay can be monitored by a second laser pulse, called probe pulse, that transfers population from the excited state to a detectable state, *i.e.* another excited or an ionic state. In figure 1.3 (and 1.4 and 1.5) the state
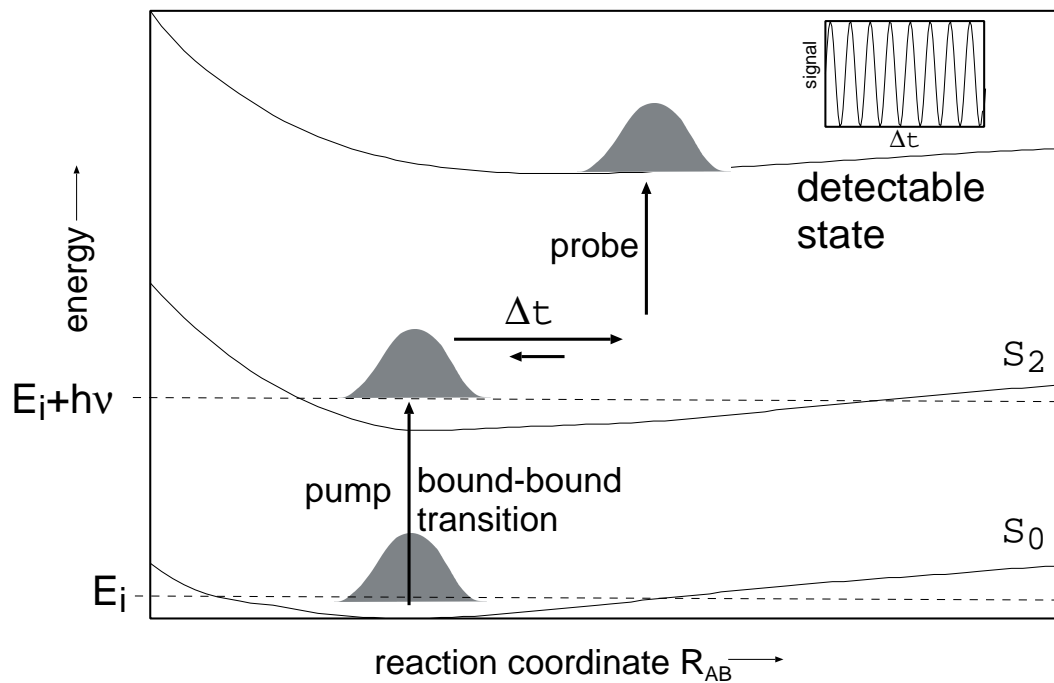
Figure 1.4: *A bound-bound ($S_0 \rightarrow S_2$) transition leads to a vibrational structure of the pump-probe signal (E_i = initial energy, $h\nu$ = pump photon energy).*

of the molecule is visualized by representative wave packets moving on and carrying out transitions between the potential energy curves.

The molecule will not decay if the ground state wave packet is transferred to quasi-bound state (in figure 1.4 the second lowest energy excited, singlet state S_2), where the wave packet is trapped (bound-bound transition). The resulting pump-probe signal shows a vibrational pattern which reflects the vibrational motion of the wave packet in the excited state.

If, however, the bound state S_2 is coupled to a repulsive state S_1, the molecule can decay via Internal Conversion (IC), as depicted in figure 1.5. The wave packet vibrating in the bound S_2 state releases population each time it reaches the (non-adiabatic) crossing point where the coupling is strongest. Consequently, the pump-probe spectrum shows a decaying signal with a superimposed vibrational pattern. The decay time can be determined by fitting an exponential multiplied by a cosine function to the pump-probe signal and it will be governed by the strength of the coupling between the S_1 and S_2 state. This type of UV photodissociation is called electronic predissociation or Herzberg's type I predissociation. If the excited state has a well at close distances and a barrier blocks the dissociation channel, the excited state wave packet can decay either by tunneling or by IVR. The latter type of decay is called Vibrational or Herzberg's type II predissociation.
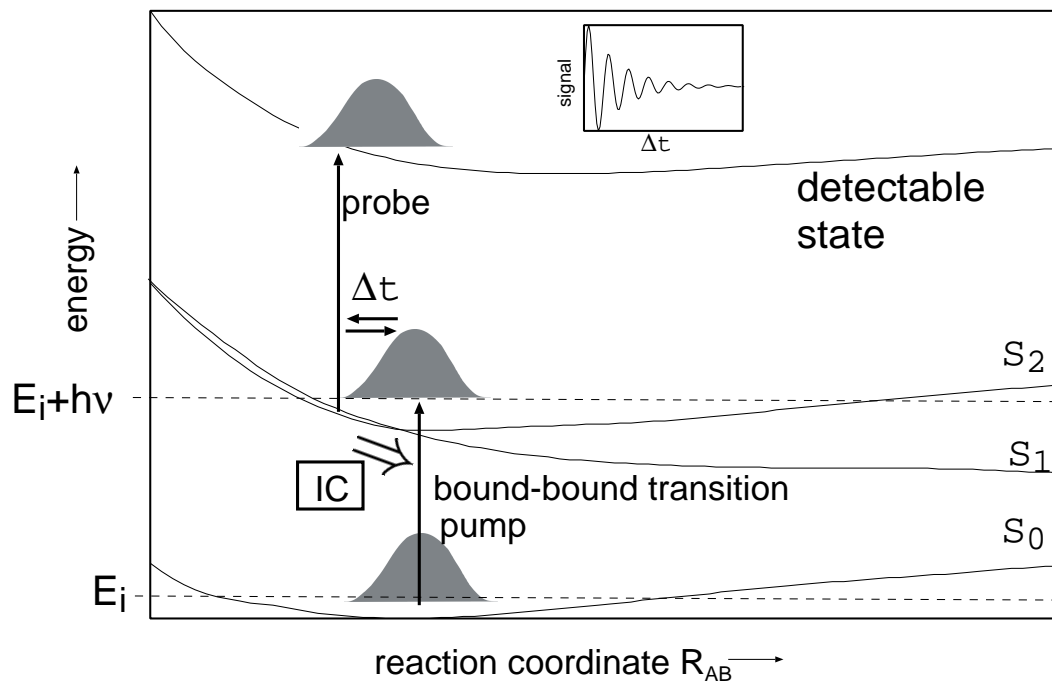
Figure 1.5: *Electronic (or Herzberg's type I) predissociation: The quasi-bound S_2 state is coupled with the repulsive S_1 state. Population is transferred to the repulsive state by Internal Conversion (IC). The pump-probe spectrum shows a decaying signal with a vibrational pattern (E_i = initial energy, $h\nu$ = pump photon energy).*

1.2 Experimental background and one-dimensional model

1.2.1 Photochemistry of CpMn(CO)$_3$

Metal carbonyl complexes are among the most photoreactive transition metal complexes known. Possible photoprocesses include electronic absorption, luminiscence, nonradiative decay, energy transfer, and photochemical reactions. In solution, the dominant photoreaction of CpMn(CO)$_3$ is the loss of CO, which leads to the monosubstituted products [42]:

$$CpMn(CO)_3 + L \overset{h\nu}{\rightarrow} CpMn(CO)_2L + CO. \tag{1.4}$$

Equation (1.4) will proceed for any L having nucleophilic character, *e.g.* the quantum yield for (1.4) is 1.0 for L = acetone [42]. High temperatures are required to thermally substitute CO by another ligand L in CpMn(CO)$_3$, whereas the photochemically substitution proceeds at room temperature. Thus, the absorption of a photon leads to an excited state where the Mn-CO bond is weakened and the chemical reactivity with respect to substitution of the CO group is enhanced
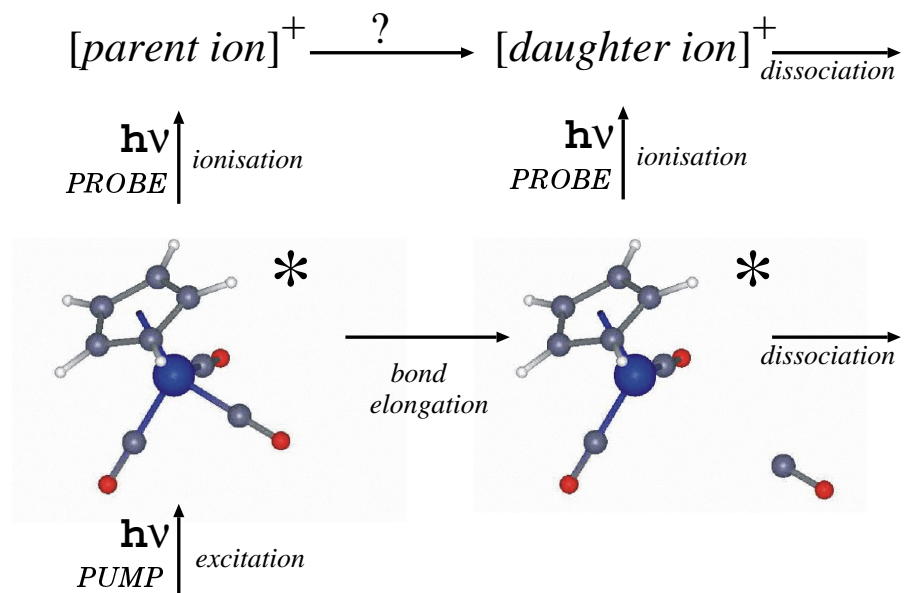
Figure 1.6: *Reaction scheme: After excitation of CpMn(CO)₃ by the pump laser, the excited state may be probed to an ionic state at different Mn-CO distances depending on the shape of the excited states potential.*

[39]. The primary unimolecular process of reaction (1.4) is the photodissociation of $CpMn(CO)_3$ which can formally be written as (see equations 1.1 and 1.2):

$$CpMn(CO)_3 + \hbar\omega \overset{(I)}{\rightarrow} \left(CpMn(CO)_3\right)^* \overset{(II)}{\rightarrow} CpMn(CO)_2 + CO. \qquad (1.5)$$
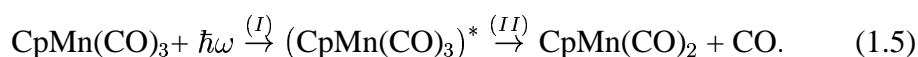
The first step (I) indicates absorption of a photon with energy $\hbar\omega$. The second step (II) implies the decay of the excited molecule $CpMn(CO)_3^*$ leading to the fragments $CpMn(CO)_2$ and CO. This unimolecular process (II) governs the velocity of the overall photodissociation process.

In this work photodissociation and ionization of the half-sandwich [39, 43] complex $CpMn(CO)_3$ is investigated in the gas phase. Different excited states are involved in the first step (I) of equation (1.5) depending on the parameters of the first (=pump) pulse. The second pulse (= probe) then ionizes the molecule leading either to the parent ion $CpMn(CO)_3^+$ or to the fragment (=daughter) ion $CpMn(CO)_2^+$ plus one CO ligand.

In figure 1.6 the different processes that may occur in the pump-probe ionization experiment are sketched. Two mechanisms are formally possible with respect to the production of the fragment ions:

1. The molecule can be first ionized and than fragmented: For instance, probing an excited state at small internuclear distances to a repulsive ionic state leads to the daughter ion. If the probed ionic state is bound the parent ion is produced.

2. A dissociative excited state can first lead to the fragments which can be then ionized: For instance, the molecule is excited to a repulsive excited state which is probed after bond elongation. The probed ionic state decays to the fragments if the kinetic energy suffices to overcome the ionic states barrier, or if the ionic state is repulsive.

In general, other mechanisms "intermediate" between 1. and 2. are also possible.

1.2.2 Experimental structure of CpMn(CO)$_3$ and UV-spectrum

Little information is found in the literature about the gas-phase structure of CpMn(CO)$_3$. Extended Hückel calculations predict a very small barrier to rotation for cyclopentadienyl(Cp)-M(CO)$_3$ transition metal complexes, 0.002 kcal/mol (0.0084 kJ mol^{-1}) [44]. At 70°C a freely rotating Mn(CO)$_3$-group with respect to the Cp ring and a staggered conformation as the one depicted in figure 1.7 (a) are in agreement with gas-phase electron diffraction studies by Almond et. al. [45]. At
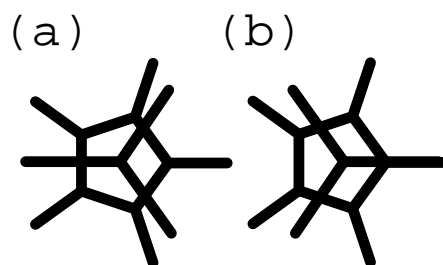

Figure 1.7: *Staggered (a) vs. eclipsed (b) C$_S$ structure of η_5-CpMn(CO)$_3$: At low temperatures (a) should be preferred .*

low temperatures, like in molecular beams, the Mn(CO)$_3$-group should not rotate with respect to the Cp ring and the three equivalent carbonyl groups should, for sterical reasons, lie in a staggered conformation (cf. figure 1.7(a)). Therefore, in our calculations, we assume a C$_S$ symmetry of the whole "staggered" molecule, CpMn(CO)$_3$, with local symmetries C$_{3v}$ and D$_{5h}$ of the Mn(CO)$_3$ and Cp fragments, respectively (*cf* figure 1.7 (a)). This assumption is justified within experimental error. [2]

The experimental UV spectrum [46] shown in figure 1.8 presents two bands, one around 340 nm (3.65 eV) and another one at around 250 nm (4.96 eV) with

---

[2]For instance, Fitzpatrick et. al. [47] observed a crystal structure where the Cp ring possesses symmetry approaching C$_{2v}$.
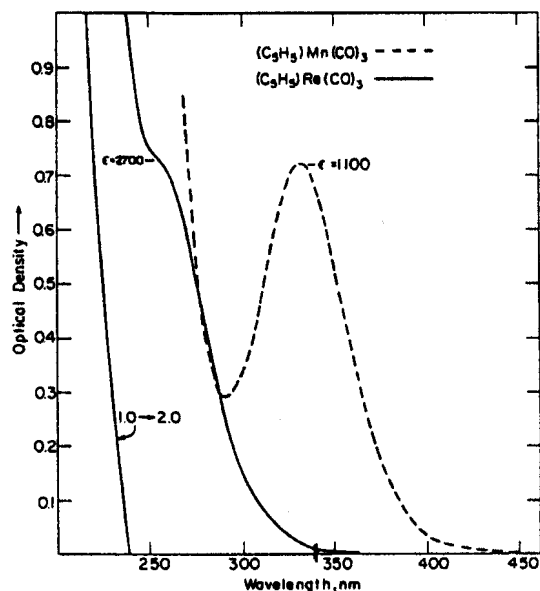
Figure 1.8: *Experimental UV spectrum of CpMn(CO)₃ [46] .*

onset at 300 nm (4.13 eV). The electronic ground state of $CpMn(CO)_3$ is charac-
terized by the occupation of the five 3d-orbitals centered at the manganese atom
[37]: Three of them are doubly occupied and constitute the three highest occupied
orbitals of the molecule whereas the other two are empty being the lowest unoccu-
pied orbitals. Assuming a pseudo-"O_h" symmetry of $CpMn(CO)_3$ the occupied d-
orbitals have "t_{2g}" and the unoccupied orbitals have "e_g" symmetry. Consequently,
the first band in the UV spectrum (*cf* figure 1.8) can be assigned to a d-d (LF) trans-
ition [46].

1.2.3 Pump-probe experiments

Figure 1.9 shows a series of pump-probe spectra, which were recorded on the mass
peaks of the parent ion $CpMn(CO)_3^+$ and the following fragment ions $CpMn(CO)_2^+$,
$CpMn(CO)^+$ and $CpMn^+$ [24, 27, 28]. The full lines indicate numerical fits to the
recorded data obtained by a deconvolution algorithm. The resulting decay times
and the time shifts of the transient signal maxima are also given. The results in-
dicate - as already observed by Trushin et al. [48, 49] - a progressive shift of the
observed ion transients. This provides evidence for a consecutive population of
several neutral precursors, each one having its own ionic fragmentation pattern
of progressively less ligands. The pump probe signals depicted in figure 1.9 have
been measured using pump laser pulses with a full width at half maximum of about
110 fs at 400 nm for the excitation and $\approx$ 90 fs probe pulses centered at 800 nm
for the ionization process. Recently performed pump-probe spectra with $\approx$ 40 fs

pump and probe pulses will be presented and discussed in section 4.5.

An accurate *ab initio* description of the whole fragmentation cascade including the loss of all the ligands and many degrees of freedom is not possible with nowaday methods and computer capability. Consequently, only the loss of the first CO ligand with an experimental decay time of 66 fs will be simulated in this work by *ab initio* quantum chemistry and dynamics.
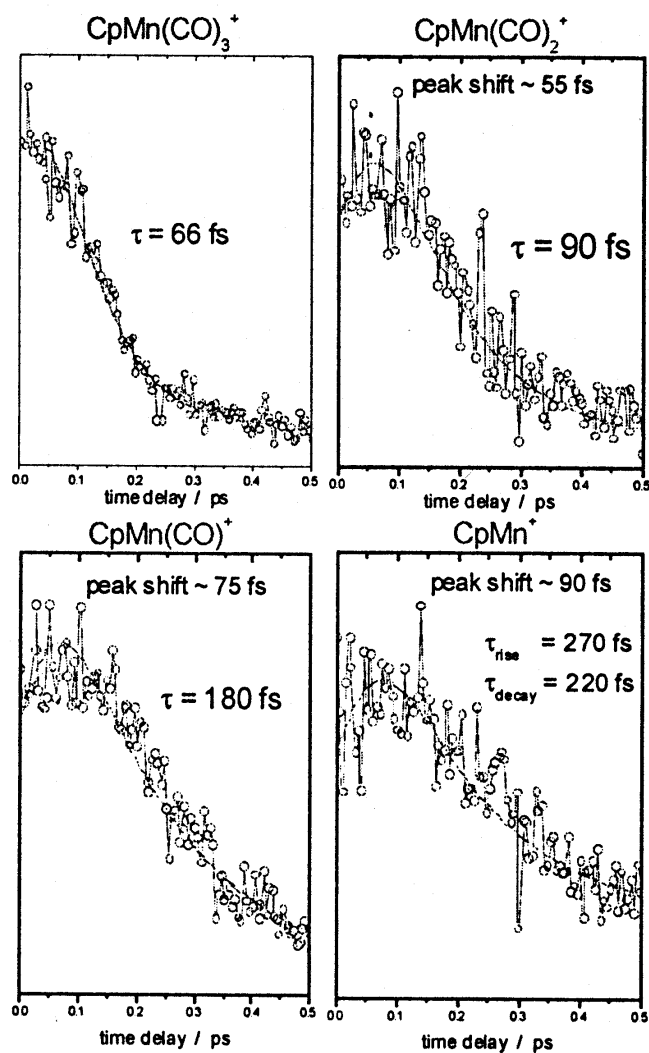

Figure 1.9: *Experimental pump-probe spectra of CpMn(CO)₃ [28] .*